Microstructure and Precipitate Evolution in Cu-3.2Ni-0.75Si Alloy Processed by Twin-Roll Strip Casting

Guangming Cao, Shuang Zhang, Jian Chen, Fei Jia, Feng Fang, and Chenggang Li

Given the sub-rapid solidification characteristics of twin-roll strip casting (TRSC), the solidification structure and growth process of precipitates during aging treatment were studied. The results showed that TRSC could refine the solidification structure and inhibit the microsegregation of Cu-3.2Ni-0.75Si alloy. During aging treatment, the precipitates mainly consisted of rod β-Ni_3Si and disk δ-Ni_2Si. The precipitate size was increased by increasing the aging time, which altered the mechanism of precipitation strengthening. Also, the experimental results indicated that precipitate strengthening arises either from the cutover mechanism or from the Orowan mechanism. Furthermore, the Avrami equation, which describes the kinetics of phase transformation and electrical conductivity during aging were established for the Cu-Ni-Si alloy, and the calculated results are consistent with the data. The Cu-3.2Ni-0.75Si alloy after aging treatment at 450 °C for 4 h exhibited optimum performance, and the tensile strength and electrical conductivity were as high as 711 MPa and 43.2% IACS, respectively.

1. Introduction

The Cu-Ni-Si alloy is a structural and functional material and can be widely used in electrical connectors, lead frames, and electronic packaging owing to its outstanding properties (Ref 1-3). To surmount the strength and conductivity trade-off dilemma, it is essential to achieve nanometer-sized precipitates during aging treatment (Ref 4-7). Furthermore, adding Ni provides excellent heat stability compared to other types of Cu alloys (Ref 8, 9). Gholami et al. (Ref 10) studied the effects of grain refinement on the phase transformation kinetics of Cu-Ni-Si alloys, and maximum strength at 6 and 12 h was obtained for ultrafine-grained and coarse-grained Cu-Ni-Si alloys, respectively. Lee et al. (Ref 11) investigated the precipitation behavior of Cu-Ni-Si alloys, and demonstrated achieving synergistic strengthening by grain refinement and fine precipitates; meanwhile, high electrical conductivity was retained. Wu (Ref 12) also studied the correlation between microstructure and properties of Cu-Ni-Si alloys and suggested that both the degree of precipitate and tensile strength were improved simultaneously during aging treatment. Jia (Ref 13) explored the morphology and orientation of δ-Ni_2Si precipitates and disclosed that many disk-shaped δ-Ni_2Si precipitates were uniformly distributed over Cu-Ni-Si alloys and δ-Ni_2Si precipitates demonstrated an orthogonal structure. The microstructural characteristics of Cu-Ni-Si alloys during aging were systematically studied by few researchers, providing useful theoretical guidance during processing of high-performance Cu-Ni-Si alloys (Ref 10-13). However, a few studies have focused on the coarse grain and severe microsegregation of the solidification structure of Cu-Ni-Si alloys, which were obtained through slow cooling. Based on the above results, an improvement in the properties of Cu-Ni-Si alloys is severely limited in the conventional processes (Ref 10, 11, 14). Fortunately, twin-roll strip casting (TRSC), a sub-rapid solidification technology, has been successfully used to fabricate a variety of metals. Liu et al. (Ref 15) successfully prepared 17% Cr ferritic stainless steel (FSS) cast strip (CS) by TRSC at different melt superheating, and the as-cast structure of FSS CS was composed of fine equiaxed and columnar grains. Zhao et al. (Ref 16) effectively developed TRIP-aided lean duplex stainless steel by TRSC. Interestingly, the as-cast CS consisted of fine Widmanstatten structure and equiaxed crystals on account of sub-rapid cooling rate. Daamen et al. (Ref 17) also pointed out that TRSC is an option to produce TWIP steels with competitive tensile strength compared to TWIP steels obtained through the conventional processing methods. All these studies revealed that TRSC is beneficial to refine microstructure as well as inhibit segregation.

The present work aims at fabricating a high-performance Cu-Ni-Si alloy utilizing TRSC. The Cu-3.2Ni-0.75Si alloy was processed using strip casting, solution treatment, cold rolling, and aging treatment. Also, the evolution of precipitates and electrical conductivity was investigated in detail.

2. Experimental Materials and Methods

The 3.0-mm-thick Cu-3.2 wt.%Ni-0.75 wt.%Si alloy was cast by a vertical type twin-roll strip caster having internally water-cooled copper rolls superheated at 30 °C and then water-cooled to room temperature. The speed of the casting roll was

Guangming Cao, Shuang Zhang, Jian Chen, Fei Jia, Feng Fang, and **Chenggang Li**, The State Key Laboratory of Rolling and Automation, Northeastern University, Shenyang 110819, China. Contact e-mail: caogm@ral.neu.edu.cn.

30 m/min. The strip was subjected to a solution treatment at 900 °C for 0.5 h, followed by cold rolling to 0.3 mm thickness and aging at 300-500 °C for 0.5-8 h.

Grain size distribution analysis was conducted using Zeiss Ultra 55 field emission scanning electron microscopy (FE-SEM). The samples were prepared by conventional electrolytic polishing using 70% H_3PO_4 + 30% H_2O (volume fraction). Element segregation behavior was observed in a JEOL JXA-8530F electron probe microanalyzer (EPMA). The microstructure and precipitate morphology were examined in a transmission electron microscope (TEM, Tecnai G^2 F20), where the samples were prepared by double jet electrolytic polishing in a bath kept at 30 °C and containing 30% nitric acid and 70% methanol (volume fraction). The tensile test was carried out on CMT5105-SANS tensile machine from three test samples. The gauge length of tensile samples was 25 mm, and the tensile rate was 2 mm/min. The electrical conductivity at room temperature was measured by a ZY9987 digital micro-ohmmeter, where the sample length exceeded 100 mm. The measured error was less than 1 μΩ, and there were five test samples.

3. Experimental Results

3.1 Microstructure and Microsegregation of Initial as-Cast Strip

The microstructure of the as-cast strip is shown in Fig. 1. The electron backscattered diffraction (EBSD) data revealed a mixed structure consisting of coarsened equiaxed grains in the surface layer and fine equiaxed grains in the central layer. The grain size varied from 5 to 200 μm, and the mean size was about 100 μm. The grains were found to be refined as compared to that of conventional ingot (Ref 18-21). The formation of fine equiaxed crystal zone in the center is linked to the unique forming process of TRSC. The casting strip must bear the rolling force during solidification. Some solidified grains may be crushed to act as nucleation sites of the solid metal melt in the central layer (Ref 16, 17). Therefore, the solidification structure of the as-cast strip is characterized by coarse equiaxed grains in the surface layer and fine equiaxed grains in the central layer.

Figure 2 presents Ni and Si distributions of the as-cast strip and solution specimen. The Ni and Si segregate at grain boundaries, as shown in Fig. 3(a). Also, this microsegregation can be eliminated after subjected to a solution treatment for 0.5 h, indicating that the solution treatment time can be significantly shortened in TRSC compared to conventional processing. Generally, during the process of solidification, the grain boundary segregation is related to solute redistribution. The degree of solute redistribution in the solid and liquid phases is also related to the cooling rate (Ref 22). The sub-rapid solidification characteristics of TRSC can considerably improve the initial nucleation undercooling of molten metal which causes the atomic clusters in the liquid phase to obtain a higher nucleation and growth rates. As a result, finer solidification structure with weaker element segregation is formed during sub-rapid solidification. Based on the above analysis, TRSC offers an encouraging microstructure to further improve the properties of Cu-3.2Ni-0.75Si alloy through the incorporation of subsequent aging treatment.

3.2 Microstructure Evolution During Aging

Figure 3 shows the microstructure of the samples aged at 400, 450, and 500 °C for 3 h. When the alloy was aged at 400 °C, the diffusion rate of atoms was slow, and the degree of recovery was weak. Thus, shear band and deformation structure produced by cold rolling are still visible (Fig. 3a). When the alloy was aged at 450 °C, shear band and deformation structure were decreased while the precipitation rate was increased. Fine precipitates were gradually reached the saturation level and were uniformly distributed at grain boundaries, as shown by white arrows in Fig. 3(d). When the aging temperature reached 500 °C, the coarsened recrystallized grains and precipitates were observed, and the size of some of the precipitates reached between 0.4 and 0.5 μm, as shown by the white arrow in Fig. 3(f).

Figure 4 displays the microstructure of the samples aged at 450 °C for 2, 4, and 6 h. With an increase in the aging time, the alloy does not experience recovery and recrystallization, and the fibrous structure formed by plastic deformation could still be noted in Fig. 4(a), (c), and (e). The size of the precipitates grew substantially to 0.7–0.8 μm for 6 h of aging, as shown in Fig. 4(f).
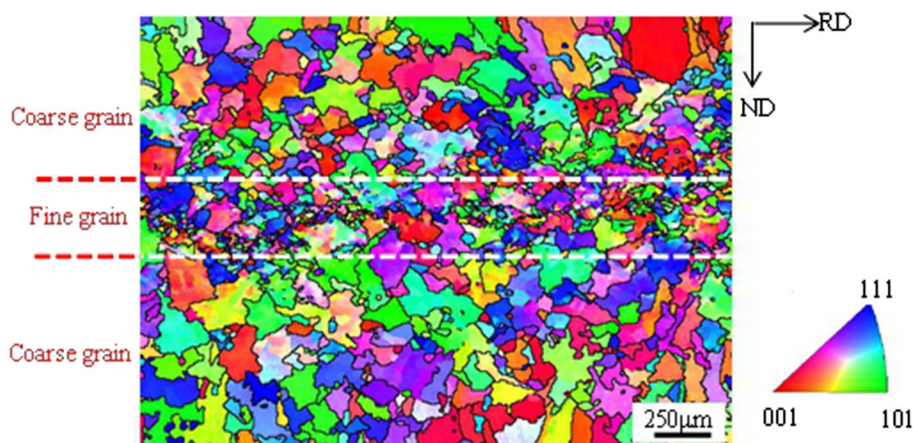
Fig. 1 EBSD orientation map of the experimental Cu-3.2Ni-0.75Si alloy
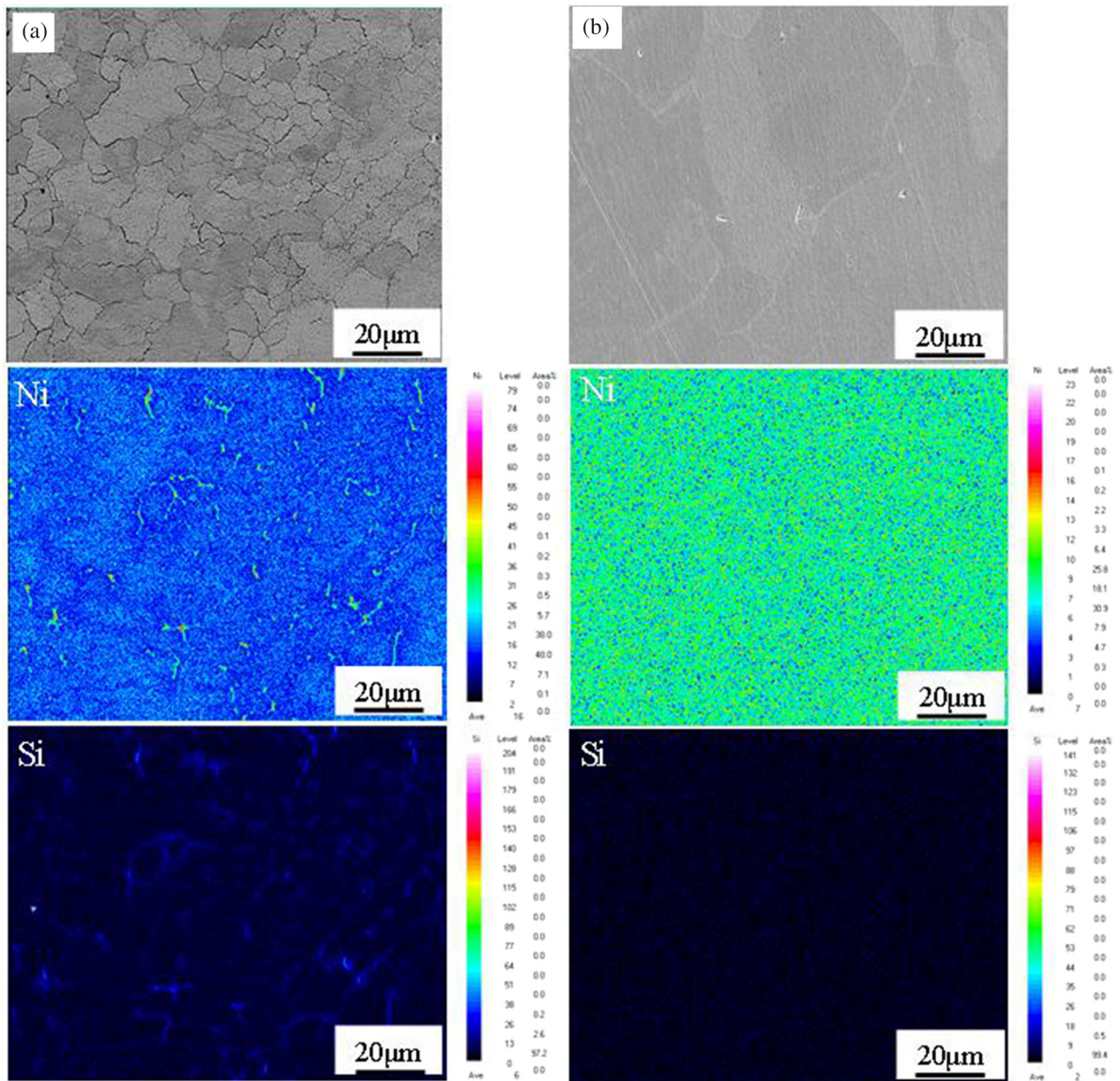
Fig. 2 Elemental maps for the as-cast strip and solution specimen (a) as-cast strip and (b) solid solution at 900 °C for 0.5 h

3.3 Conductivity Measurements

The tensile curves of Cu-3.2Ni-0.75Si alloy after aging are displayed in Fig. 5. And the effect of aging temperature on electrical conductivity and tensile strength of the alloy is displayed in Fig. 6. As the aging temperature was increased, both the tensile strength and electrical conductivity also increased rapidly. The peak temperature of hardening is around 450 °C, after which the tensile strength began to decrease with a further increase in the aging temperature, while electrical conductivity increased gradually. At the peak temperature of hardening, the effect of aging time on electrical conductivity and tensile strength of the alloy is shown in Fig. 7. With an increase in the aging time, both tensile strength and electrical conductivity increased quickly. The peak time of hardening was around 4 h, and the tensile strength and electrical conductivity were 711 MPa and 43.2% IACS, respectively. When the aging

time was greater than 4 h, overaging occurred, tensile strength decreased sharply, and the increasing trend of electrical conductivity was slowed down.

A comparison of the properties of different elastic coppers (Ref 21) and the alloy obtained in this study are shown in Fig. 8. The TRSC can improve the tensile strength and conductivity of Cu-3.2Ni-0.75Si alloy under the conditions of similar components and hence can exhibit a promising prospect in replacing the casting process.

3.4 Correlation Between the Microstructure and Properties of Cu-3.2Ni-0.75Si Alloy

The microstructural evolution and precipitation behavior of the alloy during aging influence the macroscopic properties. During aging at 300–450 °C, with an increase in temperature, on the one hand, the diffusion rate of atoms gradually increases,
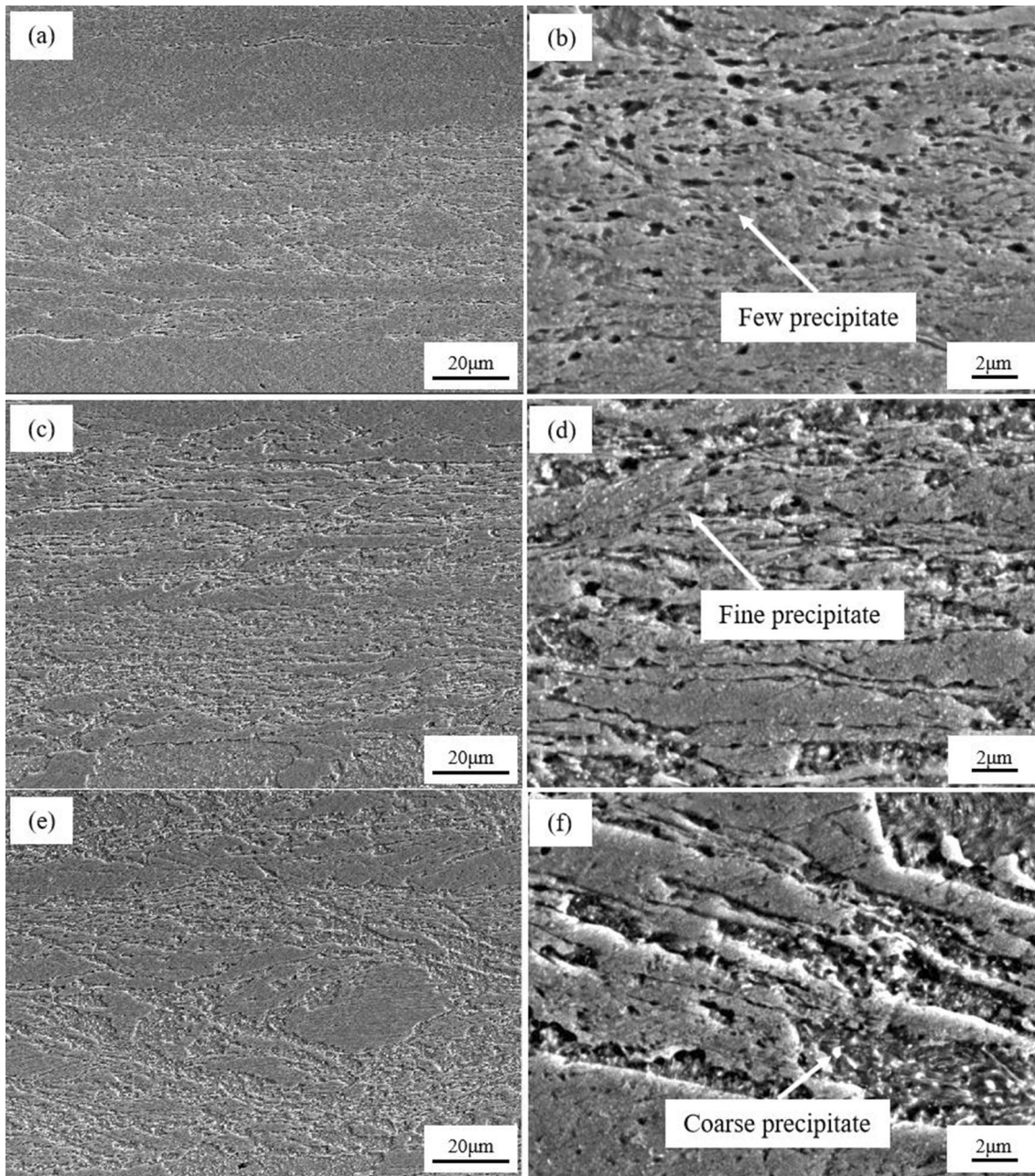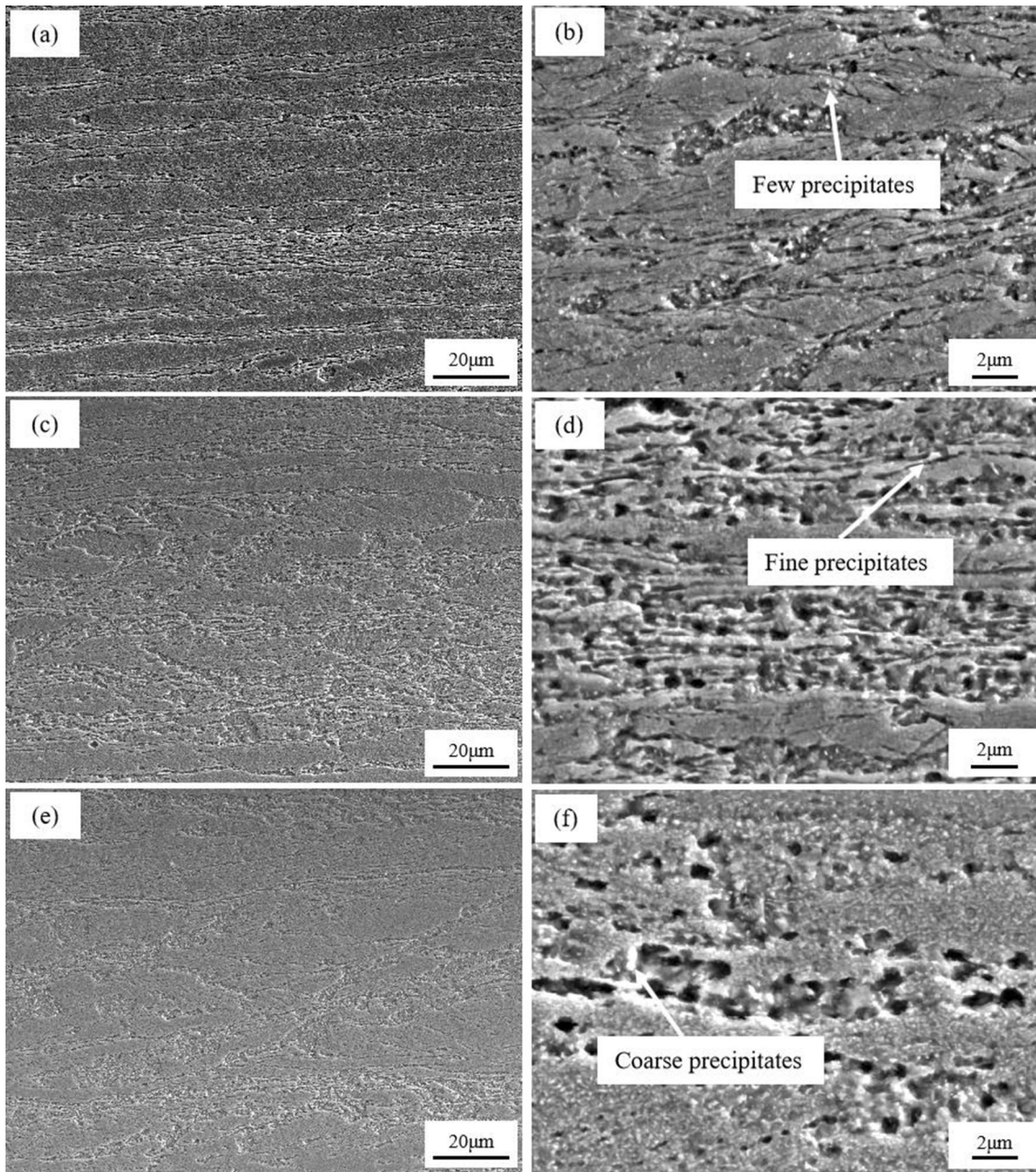
Fig. 3 Microstructural evolution of Cu-3.2Ni-0.75Si alloy aged at (a, b) 400 °C, (c, d) 450 °C, and (e, f) 500 °C for 3 h

rapid recovery occurs in the matrix, and residual supersaturated vacancy produced by the solution treatment significantly reduces, resulting in a decrease in the scattering of electrons. On the other hand, the stored energy accumulated by plastic deformation is rapidly released. As a result, alloying elements dissolved in the matrix precipitate and uniformly distribute at the grain boundaries, which effectively hinders dislocation migration and purifies the matrix (Ref 23-25). The tensile strength and conductivity of the alloy during the process of aging at 300–450 °C increased rapidly. When the aging temperature was greater than 450 °C, the recrystallized grains began to grow up, and the softening effect reduced the tensile strength of the alloy. Moreover, the precipitates began to coarsen, which lead to the weakening of the pinning ability of

precipitates to dislocation and grain boundaries (Ref 26-28). Thus, the tensile strength of the alloy was decreased.

3.5 The Microstructure of the Precipitated Phase

Figure 9 shows the TEM images of the specimens aged at 300 °C and 450 °C for 3 h. When the specimens were aged at 300 °C for 3 h, deformation bands and sub-grains produced by cold rolling were visible, as illustrated in Fig. 9(a). The formed high-density dislocations during plastic deformation provide the nucleation sites for precipitates (Fig. 9b). Also, a small amount of precipitates appears at Y-type dislocation heads, as indicated in Fig. 9(c). When the aging temperature increased to 450 °C, the recovery degree of the alloy increased, the

Fig. 4 Microstructural evolution of Cu-3.2Ni-0.75Si alloy aged at 450 °C for (a) (b) 2 h, (c) (d) 4 h, and (e) (f) 6 h

precipitation rate accelerated, and the number of precipitates increased. Figure 10 exhibits the TEM images of the specimens aged at 450 °C for 0.5 h, 4 h, and 8 h. When the specimens were aged at 450 °C for 0.5 h, a few nanometer-scale precipitates were seen (Fig. 10a). With the aging time being increased to 4 h, the number of precipitates significantly increased and was uniformly dispersed in the matrix, as shown in Fig. 10(b). A further increase in the aging time to 8 h led to overaging of the specimens, and the precipitates in the bright-field micrograph were greater than 50 nm, as revealed in Fig. 10(c). The corresponding selected area diffraction (SAD) patterns were analyzed, and two types of precipitates were identified: δ-Ni₂Si and β-Ni₃Si. δ-Ni₂Si possesses the following structural parameters: a = 0.703 nm, b = 0.499 nm, and c = 0.372 nm, whereas the structure of β-Ni₃Si is a simple

cubic lattice with a = 0.3351 nm. The phase transformation sequence of the alloy at 450 °C is: supersaturated solid solution → LI₂ ordering (Ni₃Si phase) → Ni₃Si phase → Ni₃Si phase + Ni₂Si phase. The above-observed results are consistent with the outcomes of other researchers (Ref 29-33). Through the energy spectrum analysis, it has been found that the disk shape is Ni₂Si, whereas the rod shape is Ni₃Si.

Meanwhile, twins formed during aging treatment appeared in the matrix. The emergence of twins has a positive impact on tensile strength and electrical properties of the alloy. Twins can be regarded as the internal barrier of dislocation movement, which is similar to the strengthening effect of the grain boundary. The twin boundaries that hinder dislocation movement were confirmed in situ through electron microscopic observations of the deformation process of nanocrystalline
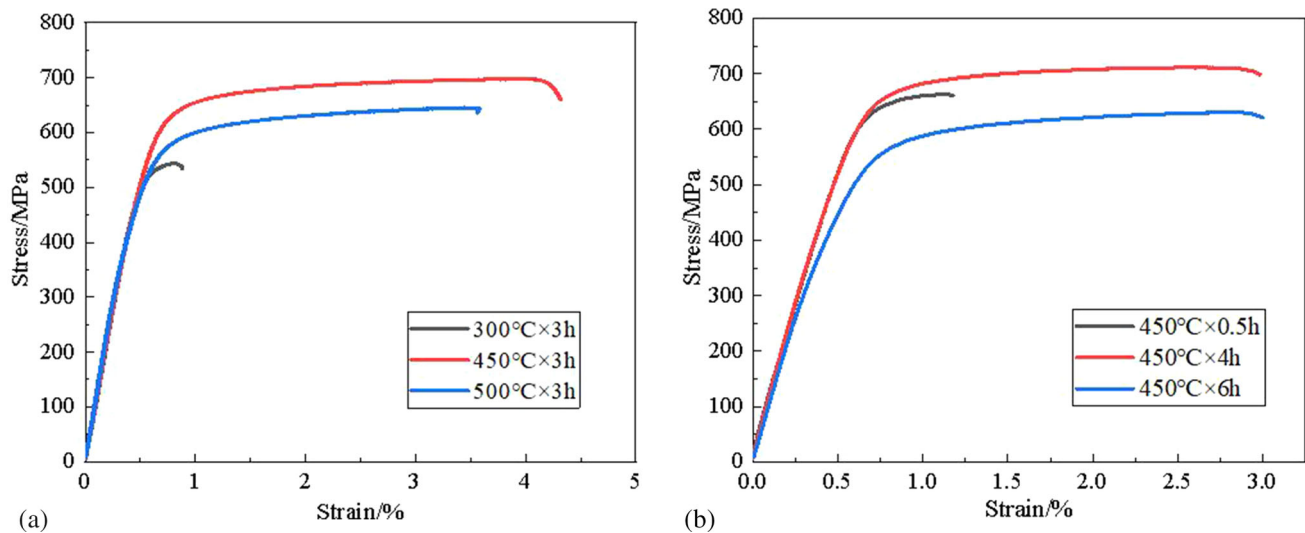
Fig. 5 Tensile curve of Cu-3.2Ni-0.75Si alloy after aging (a, b, c) 300 °C, 450 °C, and 500 °C for 3 h, (d, e, f) 450 °C for 0.5 h, 4 h, and 6 h
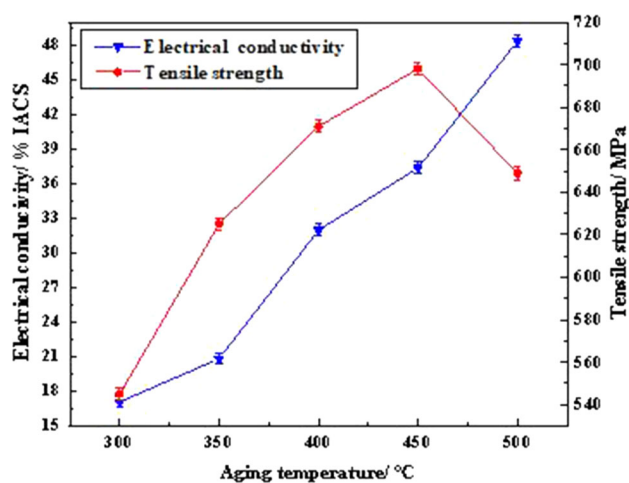

Fig. 6 Effect of aging temperature on electrical conductivity and tensile strength
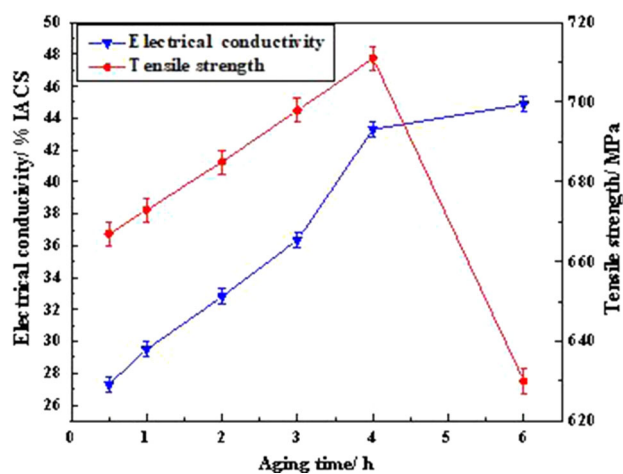

Fig. 7 Effect of aging time on electrical conductivity and tensile strength
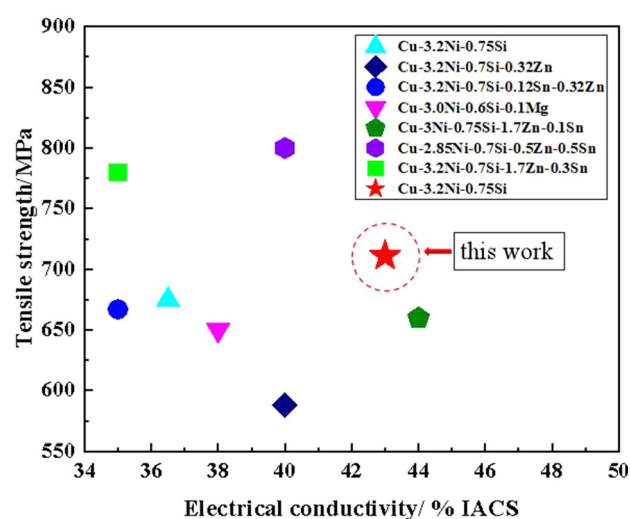

Fig. 8 Comparison of the properties between cast strip and alloy with similar components

boundaries is relatively regular, which can effectively weaken the scattering ability of free electrons (Ref 34).

4. Discussion

4.1 Precipitation Hardening Mechanism

Precipitate strengthening arises either from the cutover mechanism or from the Orowan mechanism. The cutover mechanism is responsible for coherent precipitates with small size. In contrast, the Orowan mechanism operates when the coherent precipitate size exceeds a critical value or when the precipitate is incoherent (Ref 35, 36). In the early stages of aging, the precipitates nucleate at the solute enrichment zone via spinodal decomposition. Due to a short aging time, the precipitates are relatively stable and may not grow. Dislocations can cut through smaller precipitates, leading to an increase in the surface area of the precipitates and interfacial energy. An

copper. Also, the arrangement of interfacial atoms at twin
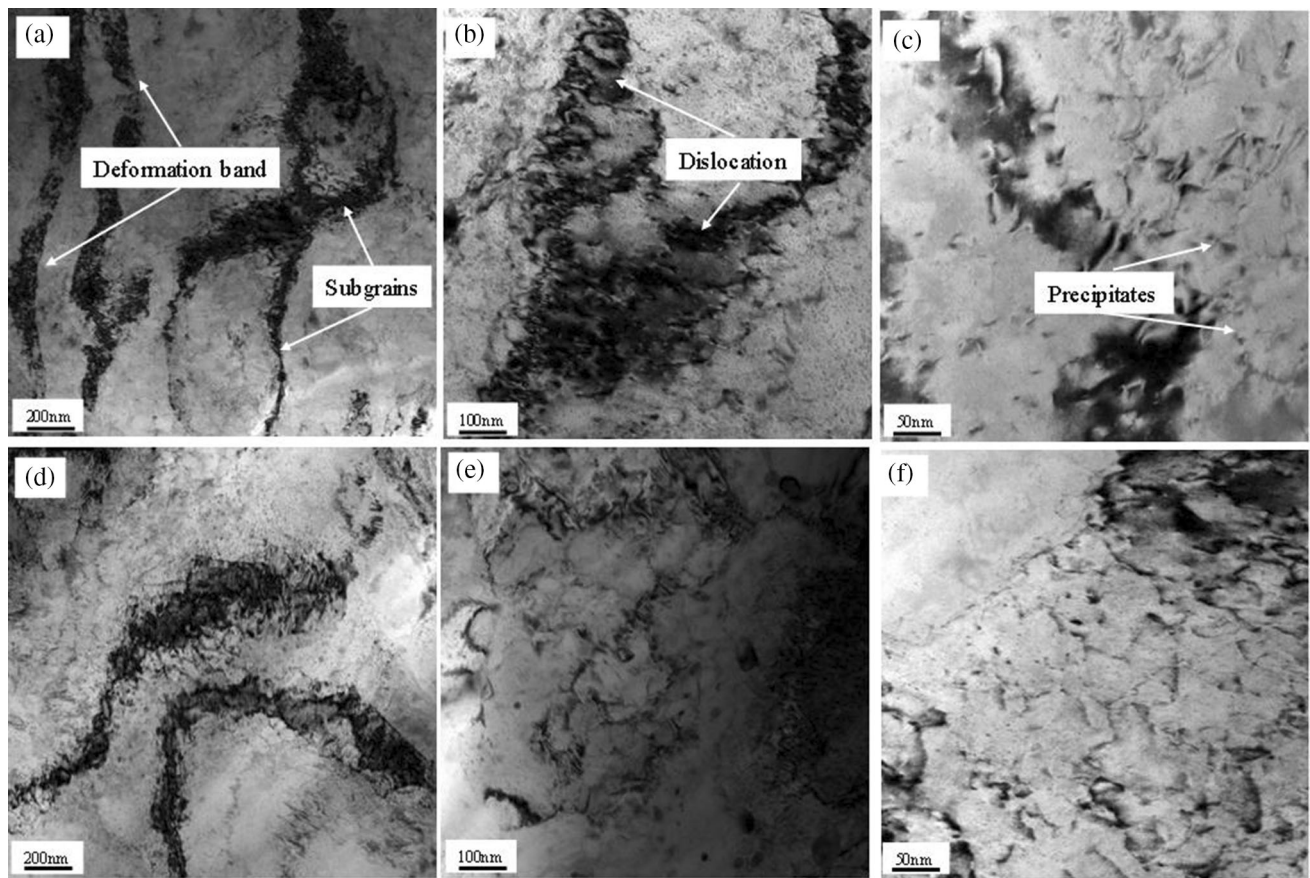
Fig. 9 TEM images of the specimens aged for 3 h (a) (b) (c) at 300 °C and (d) (e) (f) at 450 °C

increase in the strengthening can be estimated using the following Kelly-Nicholson Eq (1) (Ref 37-39).

$$\Delta\sigma = \frac{2\sqrt{b}fV_{ab}}{\pi r} \qquad (Eq\ 1)$$

where V_{ab} is the interface energy between the precipitates and matrix; b is the Bernoulli's modulus, f is the volume fraction of precipitates, and r is the radius of precipitates.

According to Eq (1), in the early stage of aging, when the radius (r) of the precipitate is small, the main factor influencing the strengthening effect is the volume fraction (f) of precipitates. Tensile strength increases with an increase in the volume fraction (f) of precipitates. The tensile strength of cold-rolled Cu-3.2Ni-0.75Si alloy was 553 MPa, and after aging at 450 °C for 0.5 h the tensile strength increased to 667 MPa. The strengthening increment was 114 MPa.

With the aging time extended to 4 h, the precipitates grew up to the critical size. The interfacial tension between the precipitates and matrix exceeded the yield strength of the matrix, resulting in the movement of misfit dislocations and the transformation of a coherent interface into a non-coherent interface. The critical size of precipitates corresponds to the peak tensile strength (Ref 34, 35). It can be seen from Fig. 7 that the tensile strength of the alloy reached its peak at 4 h. When the aging time was further prolonged, the size of precipitates exceeded the critical size, and dislocations by-passed precipitates. The strengthening increment can be estimated by the following Orowan strengthening Eq (2) (Ref 38):

$$\Delta\sigma = \frac{0.81\ MGb}{2\pi(1-v)^{1/2}} \frac{\ln(2r/b)}{\lambda} \qquad (Eq\ 2)$$

where $M = 3.06$ is the mean orientation factor for the fcc polycrystalline matrix, G is the shear modulus of the matrix, 41.0 GPa, b is the magnitude of the Burgers vector of the matrix, 0.256 nm, $v = 0.34$ is Poisson's ratio (Ref 37). λ is the effective particle spacing, and r is the radius of precipitates. In this experiment, according to the transmission results, the $\lambda = 160$ nm and $r = 25$ nm after aging at 450 °C for 4 h.

Based on Eq (2), it can be calculated that the strengthening increment was 166 MPa. It can be seen from Fig. 7 that after aging at 450 °C for 4 h, the tensile strength of the alloy was 711 MPa. And the tensile strength of cold-rolled was 553 MPa. The strengthening increment was calculated as 158 MPa. The calculated values are in good agreement with the experimental data, which proves that the Orowan mechanism plays a leading role at the peak aging stage.

4.2 Precipitation Kinetic Models

The electrical conductivity of the alloy in the aging state is extremely sensitive to the purity of the copper matrix, the size and amount of precipitates (Ref 23, 24). A part of solute atoms precipitates from the supersaturated solid solution during aging at a specific temperature. The volume fraction of precipitates, φ, can be expressed by the $V/\overline{V}$, where V is the volume fraction of precipitates per unit volume during aging for a specific time; $\overline{V}$ is the equilibrium volume of precipitates per unit volume
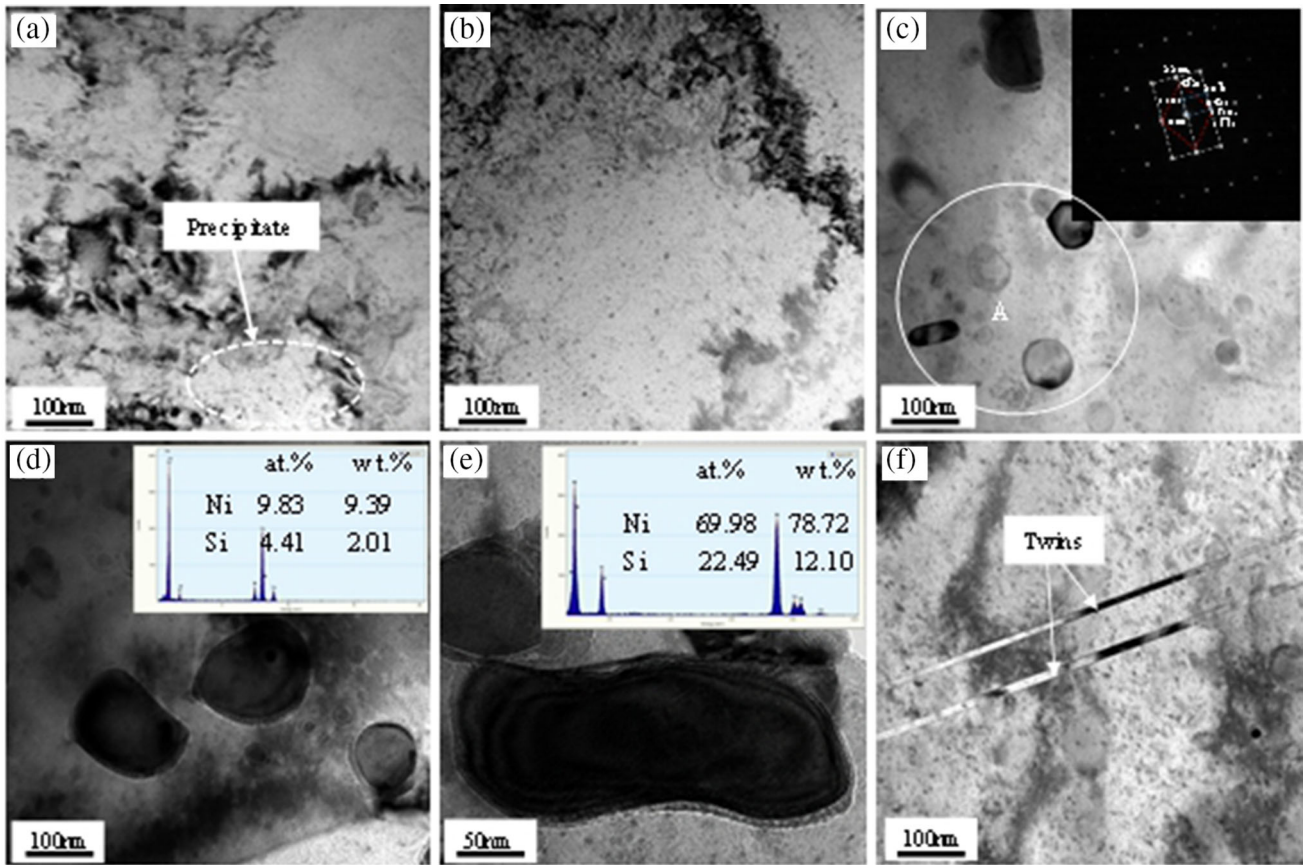
Fig. 10 TEM images of the specimens aged at 450 °C at different times (a) 0.5 h, (b) 4 h, (c) (d) (e) 8 h, and (f) formation of twins at 4 h

during aging at the same temperature for a longer time until the completion of phase transformation.

Before aging treatment, both φ and V should be zero ($V = 0$, $\varphi = 0$), and the electrical conductivity of the alloy is σ_0. After a long time, the phase transformation process completes. Hence, it is reasonable to consider V as $*V$ and φ as one ($V = *V$, $\varphi = 1$), and the electrical conductivity of the alloy is σ_{max}. σ and φ have a linear relationship according to the law of Partition, which can be expressed by following Eqs (3) and (4).

$$\sigma = \sigma_0 + (\sigma_{max} - \sigma_0)\varphi \tag{Eq 3}$$

$$\varphi = (\sigma - \sigma_0)/(\sigma_{max} - \sigma_0) \tag{Eq 4}$$

Therefore, φ can be obtained by measuring the electrical conductivity of the alloy during aging at different times. The electrical conductivity and volume fraction of precipitate Cu-Ni-Si alloy aged at 400, 450, and 500 °C for different times are shown in Fig. 11.

The kinetic Avrami equation of phase transformation can be expressed as follows (Eq 5) (Ref 10).

$$\varphi = 1 - \exp(-bt^n) \tag{Eq 5}$$

where φ is the volume fraction of precipitates, t is the aging time, and b and n are constants. b depends upon the temperature of phase transformation, the composition of supersaturated

solid solution, and size of the crystal grain. n depends on the type of phase transformation and the location of nucleation. Following Eq (5), Eq (3) can be expressed as the following electrical conductivity equation (Eq 6).

$$\sigma = \sigma_0 + (\sigma_{max} - \sigma_0)[1 - \exp(-bt^n)] \tag{Eq 6}$$

After rearranging Eq (5), following Eq (7) can be obtained.

$$1 - \varphi = \exp(-bt^n) \tag{Eq 7}$$

By taking the logarithm of both sides of Eq (7), it transforms into Eq (8).

$$\lg\left(\ln\frac{1}{1-\varphi}\right) = \lg b + n\lg t \tag{Eq 8}$$

Based on Fig. 11, the relationship between lg[Ref ln(1/1-φ)] and lg$t$ is shown in Fig. 12, and it displays approximately a straight line.

n is the slope coefficient of the line, and lgb is the intercept. The approximate values of n and b can be deduced from the straight line in Fig. 12.

The measured and calculated electrical conductivity of the alloy aged at 400, 450, and 500 °C for different times is shown in Fig. 13. The observed error is less than 4%, which is in the acceptable range. Also, the calculated results are in agreement with the experimental values.
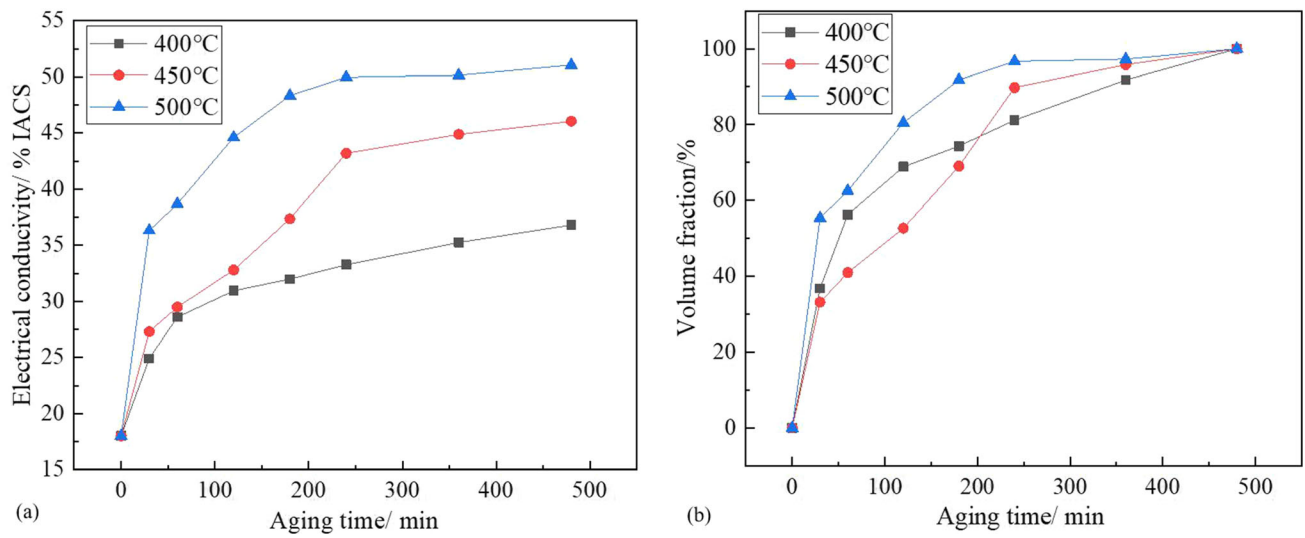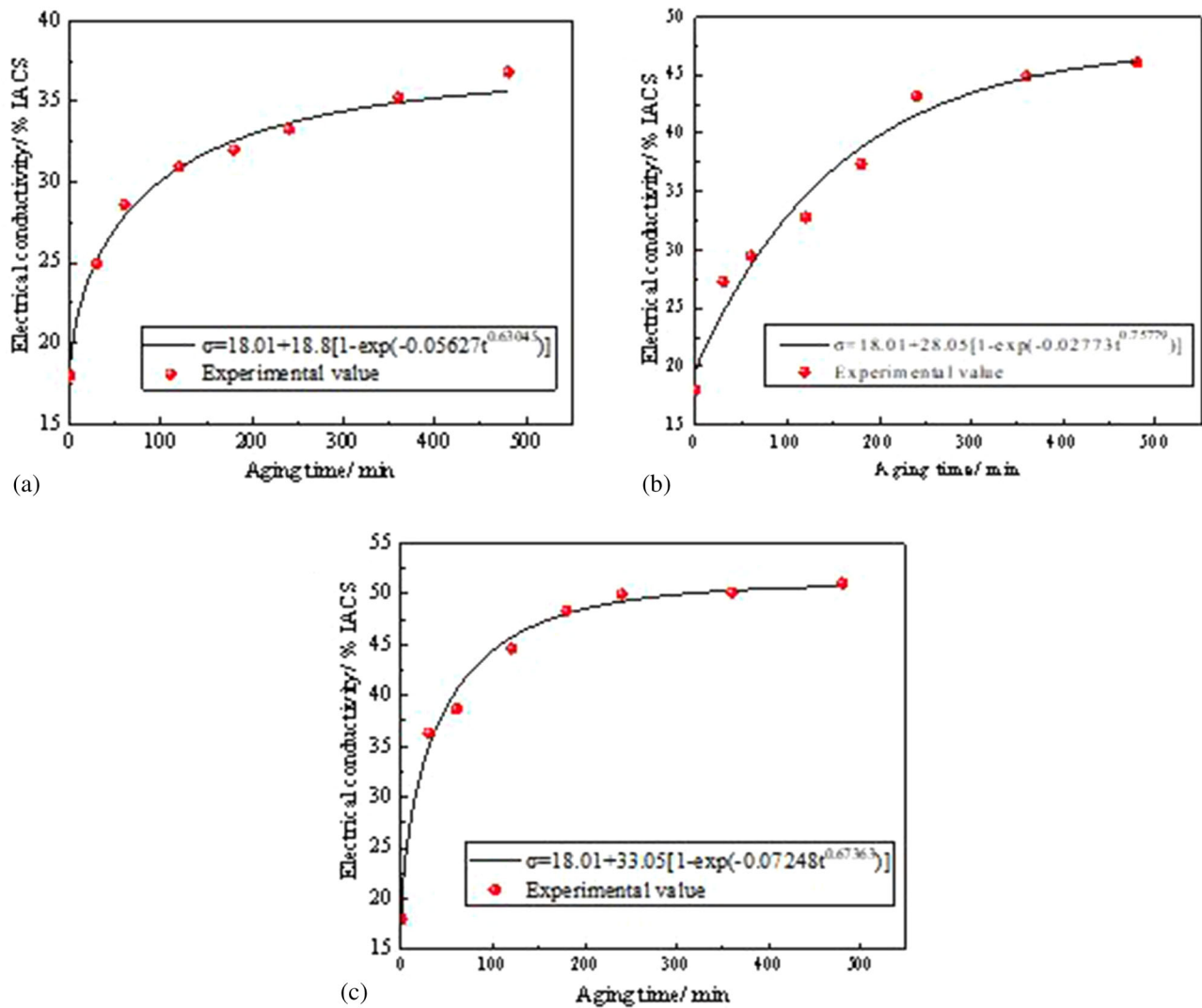
Fig. 11 Electrical conductivity and volume fraction of precipitate Cu-Ni-Si alloy aged at 400, 450, and 500 °C for different times (a) electrical conductivity and (b) volume fraction
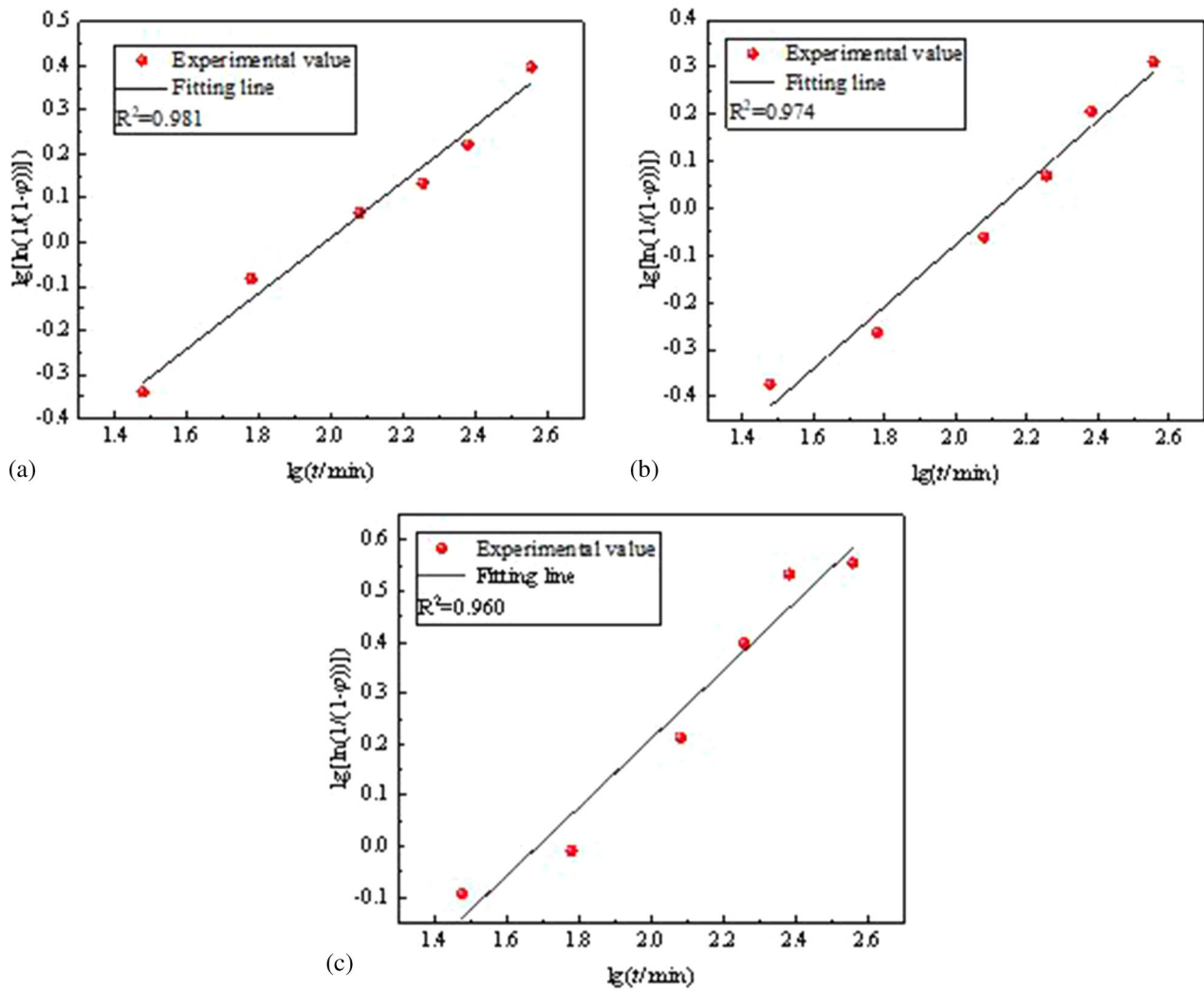
Fig. 12 Relationship between $lg[ln(1/1-\varphi)]$ and lgt of the Cu-3.2Ni-0.75Si alloy (a) 400 °C, (b) 450 °C, and (c) 500 °C

Fig. 13 Experimental and calculated electrical conductivity of the alloy aged at different temperatures (a) 400 °C, (b) 450 °C, and (c) 500 °C

The kinetic curve of precipitation is exhibited in Fig. 14. The volume fractions of precipitates increase rapidly at 500 °C and relatively slowly at 400 and 450 °C. The volume fractions of precipitates at 400, 450, and 500 °C reach 50% at aging for 60, 70, and 30 min, respectively. At 500 °C, the migration rate of elements is fast and the volume fractions of precipitates increase rapidly, which makes it easy to over age. The total amount of precipitation is low at 400 °C, so the time to reach 50% is faster. At 450 °C, the total volume fractions of precipitates are large, which is the precipitation peak temperature.

5. Conclusions

The key conclusions observed from this investigation are:

(1) TRSC can refine the solidification structure of Cu-3.2Ni-0.75Si alloy significantly, and the average grain size of the cast strip was 100 μm. Also, the solidification structure of the as-cast strip was characterized by the coarser columnar and equiaxed grains in the surface layer and fine equiaxed grains in the central layer.

(2) The microstructural analysis confirmed the presence of δ-Ni_2Si and β-Ni_3Si, which strengthens the alloy through dislocation shearing action or Orowan mechanism.

(3) The strip casting Cu-3.2Ni-0.75Si alloy aged at 450 °C for 4 h exhibited optimum performance in the tensile strength and electrical conductivity of 711 MPa and 43.2% IACS, respectively.

(4) The Avrami equation of phase transformation kinetics at 400, 450, and 500 °C was $\varphi = 1-\exp(-0.05627t^{0.63045})$, $\varphi = 1-\exp(-0.02773t^{0.75779})$, and $\varphi = 1-\exp(-0.07248t^{0.67363})$, respectively.
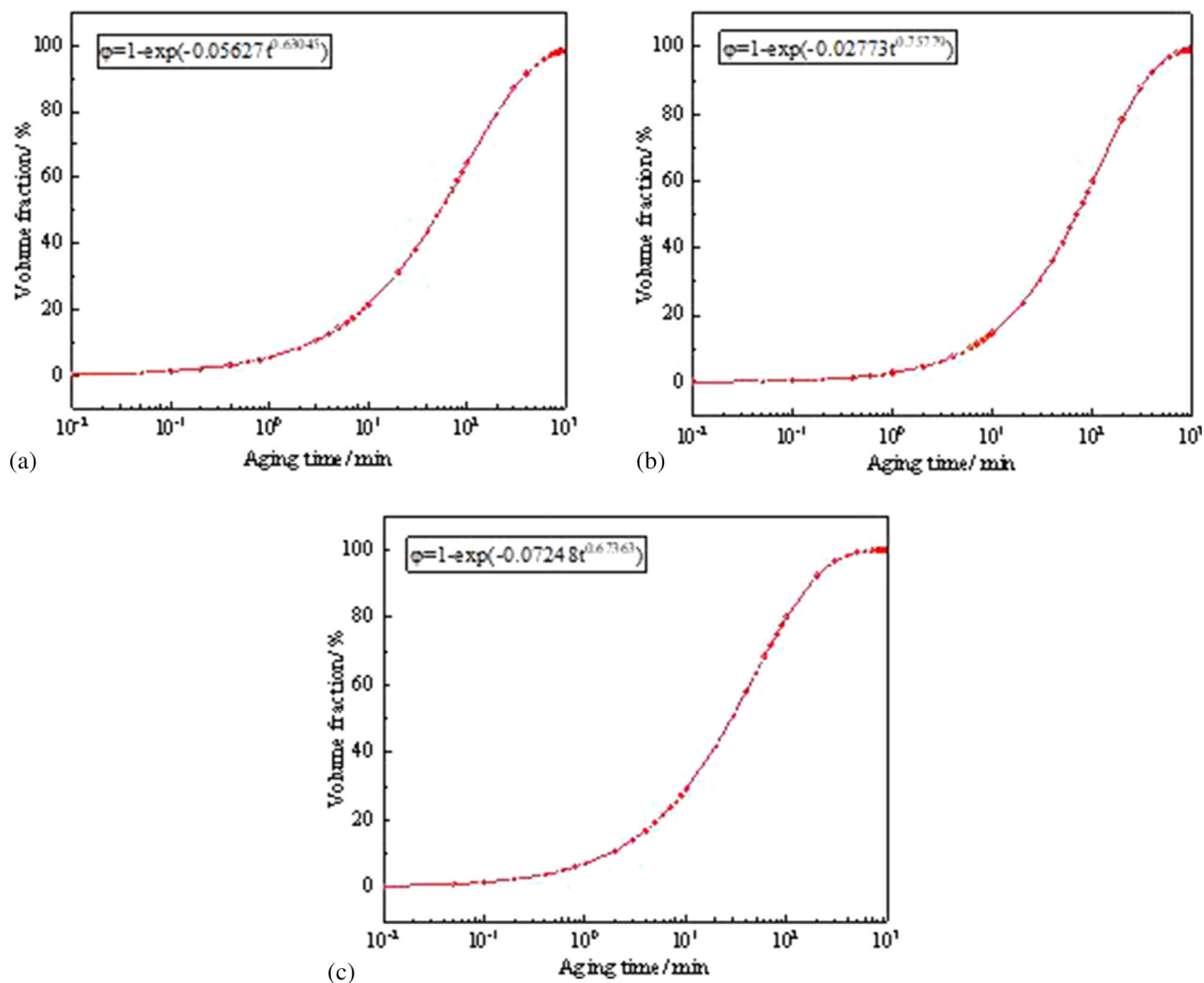
Fig. 14 Kinetic curve of phase transformation of the Cu-3.2Ni-0.75Si alloy (a) 400 °C, (b) 450 °C, and (c) 500 °C

Data Availability

The data used to support the findings of this study are included within the article.

References

1. J.Y. Cheng, B.B. Tang, F.X. Yu, and B. Shen, Evaluation of Nanoscaled Precipitates in a Cu–Ni–Si–Cr Alloy During Aging, *Alloys Compd.*, 2014, **614**, p 189–195
2. J.I. Pérez-Landazábal and V. Recarte, Nó ML, Nó ML, Determination of the Order in γ₁ Intermetallic Phase in Cu-Al-Ni Shape Memory Alloys, *Intermetallics*, 2003, **119**, p 927–930
3. D. Li, P. Franke, S. Fürtauer, D. Cupid, and H. Flandorfer, The Cu-Sn Phase Diagram Part II: New Thermodynamic Assessment, *Intermetallics*, 2013, **34**, p 148–158
4. S. Suzuki, N. Shibutani, K. Mimura, M. Isshiki, and Y. Waseda, Improvement in Strength and Electrical Conductivity of Cu-Ni-Si Alloys by Ageing and Cold Rolling, *Alloys Compd.*, 2006, **417**(1–2), p 116–120
5. B.D. Lee, H.T. Son, and J.W. Han, Microstructure and Tensile Strength on Aging Behavior of Zn Containing Mg-2Sn-0.4Mn Alloy, *Intermetallics*, 2013, **32**, p 214–218
6. H. Xie, L. Jia, and Z.L. Lu, Microstructure and Solidification Behavior of Cu-Ni-Si Alloys, *Mater. Charact.*, 2009, **60**(2), p 114–118
7. Z.Y. Pan, M.P. Wang, Z. Li, C.P. Deng, S.H. Li, and Y.L. Jia, Progress of Study of Super-High Strength Cu-Ni-Si Alloy, *Heat Treat. Met.*, 2007, **32**(7), p 55–59
8. H. Azzeddine, B. Mehdi, L. Hennet, B. Alili, M. Kawasaki, and D. Bradai, An in situ Synchrotron X-ray Diffraction Study of Precipitation Kinetics in a Severely Deformed Cu-Ni-Si Alloy, *Mater. Sci. Eng., A*, 2014, **597**, p 288–294
9. S. Suzuki, N. Shibutani, K. Mimura, M. Isshiki, and Y. Waseda, Improvement in Strength and Electrical Conductivity of Cu-Ni-Si Alloys by Ageing and Cold Rolling, *Alloys Compd.*, 2006, **417**(1–2), p 116–120
10. M. Gholami, I. Altenberger, J. Vesely, M. Wollmann, M. Janecek, and L. Wagner, Effects of Severe Plastic Deformation on Transformation Kinetics of Precipitates in CuNi3Si1Mg, *Mater. Sci. Eng., A*, 2016, **676**(676), p 156–164
11. S. Lee, H. Matsunaga, X. Sauvage, and Z. Horita, Strengthening of Cu-Ni-Si Alloy Using High-Pressure Torsion and Aging, *Mater. Charact.*, 2014, **90**, p 62–70

12. Y.K. Wu, Y. Li, J.Y. Lu, S. Tan, F. Jiang, and J. Sun, Correlations Between Microstructures and Properties of Cu-Ni-Si-Cr Alloy, *Mater. Sci. Eng., A*, 2018, **731**, p 403–412

13. Y.L. Jia, M.P. Wang, C. Chen, Q.Y. Dong, S. Wang, and Z. Li, Orientation and Diffraction Patterns of δ–Ni–2.0–Si Precipitates in Cu–Ni–Si Alloy, *Alloys Compd.*, 2013, **557**(25), p 147–151

14. Z. Li, Z.Y. Pan, Y.Y. Zhao, Z. Xiao, and M.P. Wang, Microstructure and Properties of High-Conductivity-Super-High-Strength Cu–8.0Ni–1.8Si–0.6Sn–0.15 Mg Alloy, *Mater. Res.*, 2009, **24**(6), p 2123–2129

15. H.T. Liu, Z.H. Liu, Y.Q. Qiu, G.M. Cao, C.C. Li, and G.D. Wang, Characterization of the Solidification Structure and Texture Development of Ferritic Stainless Steel Produced by Twin-roll Strip Casting, *Mater. Charact.*, 2009, **60**(1), p 79–82

16. Y. Zhao, W.N. Zhang, X. Liu, Z.Y. Liu, and G.D. Wang, Development of TRIP-aided Lean Duplex Stainless Steel by Twin-roll Strip Casting and Its Deformation Mechanism, *Mater. Trans. A*, 2016, **47**, p 6292–6303

17. M. Daamen, C. Haase, J. Dierdorf, and D.A. Molodov, Twin-roll Strip Casting: Acompetitive Alternative for the Production of High-Manganese Steels with Advanced Mechanical Properties, *Mater. Sci. Eng., A*, 2015, **627**, p 72–81

18. S. Ge, M. Isac, and R.I.L. Guthrie, Progress in Strip Casting Technologies for Steel Technical Developments, *ISIJ Int.*, 2013, **53**(5), p 729–742

19. M. Delbove, J.B. Vogt, J. Bouquerel, T. Soreau, and F. Primaux, Low Cycle Fatigue Behaviour of a Precipitation Hardened Cu-Ni-Si Alloy, *Int. J. Fatigue*, 2013, **92**, p 313–320

20. Q. Lei, Z. Li, T. Xiao, Y. Pang, Z.Q. Xiang, W.T. Qiu, and Z. Xiao, A New Ultrahigh Strength Cu-Ni-Si Alloy, *Intermetallics*, 2013, **42**, p 77–84

21. W. Wang, H.J. Kang, Z.N. Chen, Z.J. Chen, C.L. Zou, R.L. Li, G.M. Yin, and T.M. Wang, Effect of Cr and Zr Additions on Microstructure and Properties of Cu-Ni-Si Alloys, *Mater. Sci. Eng., A*, 2016, **673**, p 378–390

22. L. Strezov and J. Herbertson, Experimental Studies of Interfacial Heat Transfer and Initial Solidification Pertinent to Strip Casting, *ISIJ Int.*, 1998, **38**(9), p 959–966

23. N. Zapuskal, Effect of Coiling Operation on Strip Quality of 4.5% Si Steel in Twin-roll Casting Process, *ISIJ Int.*, 1999, **39**(5), p 463–470

24. F.J.G. Landgraf, T. Yonamine, R. Takanohashi, F.Q. Silva, J.P.V. Tosetti, and F.B. Neto, Magnetic Properties of Silicon Steel with As-cast Columnar Structure, *J. Magn. Magn. Mater.*, 2003, **254–255**, p 364–366

25. X.P. XiAO, G.J. Huang, L. Cheng, F.S. Yuan, and Y. Wu, Effect of Solution and Aging Technique on Microstructure and Properties of Cu-Ni-Si Alloy, *Chin. J. Rare Metals*, 2011, **35**(5), p 673–678

26. L. Qu, E. Wang, K. Han, X. Zuo, L. Zhang, P. Jia et al., Studies of Electrical Re-sistivity of an Annealed Cu-Fe Composite, *J. Appl. Phys.*, 2013, **113**(17), p 173–708

27. L. Tian, I. Anderson, T. Riedemann, and A. Russell, Modeling the Electrical Resistivity of Deformation Processed Metal–Metal Composites, *Acta Mater.*, 2014, **77**, p 151–161

28. L. Balogh, T. Ungár, Y. Zhao, Y. Zhu, Z. Horita, and C. Xu, Influence of Stacking-Fault Energy on Microstructural Characteristics of Ultrafine-Grain Copper and Copper–Zinc Alloys, *Acta Mater.*, 2008, **56**(4), p 809–820

29. E. Hall, The Deformation and Ageing of Mild Steel: III Discussion of Results, *Proc. Phys. Soc. Sect. B*, 1951, **64**, p 747–753

30. N. Petch, The Cleavage Strength of Polycrystals, *Iron Steel Inst.*, 1953, **174**, p 25–28

31. R.E. Kusner, J.C. Kuli, D. B. Veitch, A Copper-Nickel-Silicon-Chromium Alloy for Mold Tooling, *MoldMaking Technology*, 2007

32. Q. Lei, Z. Li, Z.Y. Pan, M.P. Wang, Z. Xiao, and C. Chen, Dynamics of Phase Transformation of Cu-Ni-Si Alloy with Super-high Strength and High Conductivity During Aging, *Trans. Nonferrous Met. Soc. China*, 2010, **20**(6), p 1006–1011

33. Q. Lei, Z. Xiao, W. Hu, B. Derby, and Z. Li, Phase Transformation Behaviors and Properties of a High Strength Cu-Ni-Si Alloy, *Mater. Sci. Eng., A*, 2017, **697**, p 37–47

34. K. Toman, The Structure of Ni_2Si, *Acta Crystallogr. A*, 1952, **3**, p p329–331

35. A.T. Dutra, P.L. Ferrandini, and R. Caram, Microstructure and Mechanical Behavior of in situ $Ni–Ni_3Si$ Composite, *Alloys Compd.*, 2007, **432**(1–2), p 167–171

36. Q. Lei, Z. Li, M.P. Wang, L. Zhang, Z. Xiao, and Y.L. Jia, The Evolution of Microstructure in Cu–8.0Ni–1.8Si–0.15 Mg Alloy During Aging, *Mater. Sci. Eng., A*, 2010, **527**(24–25), p 6728–6733

37. C.J. Youngdal, J.R. Weerman, and R.C. Hugo, Deformation Behavior in Nanocrystalline Copperr, *Scripta Mater.*, 2001, **44**(8–9), p 1475–1478

38. H. Wen, T.D. Topping, D. Isheim, D.N. Seidman, and E.J. Lavernia, Strengthening Mechanisms in a High-strength Bulk Nanostructured Cu–Zn–Al Alloy Processed via Cryomilling and Spark Plasma Sintering, *Acta Mater.*, 2013, **61**(8), p 2769–2782

39. E. Dowling Norman, Mechanical Behavior of Materials, *Mater. Today*, 2005, **8**, p 83–85